Effective utilization of unidirectional laminates for mass reduction in composite blades of multi-MW wind turbines.

ATTAR, S. and HAYAT, K.

2024

Effective utilization of unidirectional laminates for mass reduction in composite blades of multi-MW wind turbines

Suhail Attar & Khazar Hayat

Published online: 11 Dec 2024.

Submit your article to this journal ⤤

Article views: 82

View related articles ⤤

View Crossmark data ⤤

Taylor & Francis
Taylor & Francis Group

Check for updates

Effective utilization of unidirectional laminates for mass reduction in composite blades of multi-MW wind turbines

Suhail Attar [a] and Khazar Hayat[b]

[a]School of Computing, Engineering and Technology, Robert Gordon University, Garthdee Road, AB10 7GJ, Aberdeen, UK; [b]School of Mechanical Engineering, PNG University of Technology, Lae 411, Morobe, Papua New Guinea

In this study, a reduction of 7.8–10.37% in the blade mass was achieved by optimizing the thickness of unidirectional spars in the Sandia 100-m all-glass baseline blade for a 13.2 MW wind turbine. The optimized design still complies with stiffness, strength, buckling, and resonance requirements for two design load conditions (i.e. DLCs 6.2 and 1.4) specified in the IEC 61,400-1 standard for both stationary and spinning blades. A genetic algorithm was utilized to solve the multi-criteria, multi-constraint optimization problem while satisfying the allowable design limits specified by the wind turbine standard. The optimized blade designs demonstrated effective use of unidirectional laminates in the spars but led to increased tip deflection and longitudinal strains along with a decrease in buckling performance and first natural frequency.

Keywords: Genetic algorithm; large-scale composite blade; mass reduction; spar optimization

1. Introduction

The increasing size of horizontal-axis wind turbines (HAWTs) is largely motivated by the substantial growth in output power associated with longer blades, which scales with the square of blade length. Larger turbines not only enhance the efficiency of wind energy capture but also significantly lower the cost of energy production [1–5]. However, this expansion is constrained by the cubic increase in blade mass that accompanies longer blades [6].

To address this challenge, the use of lightweight fiber-reinforced plastic composites has become critical. Glass fiber reinforced plastics (GFRPs) are frequently selected for their cost-effectiveness, while carbon fiber reinforced plastics (CFRPs) offer superior strength-to-weight ratios, albeit at a higher price. As a result, many manufacturers adopt hybrid materials that combine GFRPs and CFRPs to optimize the performance and cost [7,8].

Optimizing the composite layup is essential for achieving further mass reductions, yet this task is complicated by the heterogeneous and anisotropic nature of composite materials, as well as stringent design requirements established by industry standards

[9,10]. Additionally, the wide range of loading conditions that blades experience must be carefully considered during optimization efforts.

Numerous studies have reported successful attempts at reducing blade mass through composite layup optimization. For example, a mass reduction of 8.29% was achieved in the Atlantic Orientation Corporation (AOC) blade model (7.2 m in length) by optimizing ply angles and stacking sequences [11]. However, the optimization challenges inherent in large-scale composite blades remain largely unaddressed. Other research demonstrated effective composite layup designs for a 40 m blade used in a 2 MW wind turbine, balancing cost and weight through multi-objective optimization [12,13]. Yet, many of these studies prioritize robust optimization strategies over realistic blade characteristics, limiting their practical applicability.

Investigations into spar optimization for 1.5 MW turbine blades have yielded mass reductions of 7.2%, 2.3%, and 8.5% by varying parameters such as ply numbers, thicknesses, and spar width [14–16]. Although a multi-objective optimization aimed at minimizing both mass and cost using GFRPs and CFRPs has been conducted, it similarly lacks essential specifications for real-world application [17]. In contrast, a recent study employing evolutionary and topology optimization techniques on a 28.5 m composite blade achieved an impressive 23% mass reduction without compromising structural integrity [18]. However, the applicability of these findings to larger blades remains to be validated. Additionally, gradient-based optimization studies for blades exceeding 100 m in length tend to focus on mass reduction and performance enhancement but overlook the potential for spar optimization, leaving a significant gap in the literature [19].

Several researchers have undertaken integrated aerodynamic and structural optimization to develop blades that maximize power generation while minimizing mass [20–28]. However, these coupled analyses require sophisticated tools and substantial computational resources, making the development of optimal yet practical blade layups a challenging endeavor, particularly when accounting for fabrication constraints.

The literature highlights key research gaps including a major focus on layup optimization for smaller wind turbine blades and to prioritize general optimization frameworks over practical strategies for blade mass reduction. Spar-specific optimization, particularly for large blades, remains underexplored. Studies on 1.5 MW and 2 MW turbine models suggest spar optimization can significantly reduce mass, however, the lack of detailed blade layup disclosures due to commercial constraints limits their utility. Additionally, current large-blade optimization methods emphasize overall mass reduction and/or performance enhancement, neglecting targeted strategies for components like spars, which constitute 35–40% of blade mass and offer substantial potential for optimization.

The contribution of this research is to demonstrate that the effective utilization of unidirectional laminates in the blade spar exclusively can significantly reduce the mass of composite blades in large-scale multi-MW wind turbines. This approach presents a practical and effective strategy for achieving blade mass reduction. Unlike previous works, the spar optimization is conducted on the Sandia 100 m all-glass baseline composite blade model (SNL100–00) of a 13.2 MW wind turbine, whose geometry and layup specifications are well documented and publicly available [29]. By systematically optimizing the spar design within the constraints of manufacturability, this research provides a valuable reference for future academic studies focused on reducing blade mass while maintaining structural integrity. Additionally, it directly addresses the wind turbine industry's growing demand for lightweight, cost-effective large-scale blades, ultimately contributing to a reduction in the cost of energy (COE).

The paper begins by detailing the geometry and layup of the SNL100–00 blade, followed by a discussion of the design requirements and the estimation of wind loads acting on the blade. This is complemented by a model verification process. Next, the formulation of the optimization problem is presented, focusing on spar thickness optimization under two critical design load conditions (DLCs) of 6.2 and 1.4, achieved through the genetic algorithm (GA) method, while ensuring compliance with wind turbine standard design requirements. Finally, the results and discussion are provided, leading to the conclusions at the end of the paper.

2. Large-scale composite blade model

The SNL100–00 blade is developed for a three-bladed HAWT of 13.2 MW rated power, having variable-speed and collective pitch controls for a wind speed site of class IB. The turbine rotor has maximum speed of 7.44 rpm at the rated wind speed of 11.3 m/s. A brief account of the blade geometry and its layup is discussed as following.

The blade has a 100 m length and made up of a pressure-side (PS) surface that faces the incident wind and a suction-side (SS) surface, joined together with three shear webs, i.e. leading-edge (LE) shear web, aft shear web and trailing-edge (TE) shear web as shown in the blade planform in Figure 1. Each surface can be divided into four panel regions: LE panel, spar, aft-panel and TE reinforced panel as depicted in the cross-section view A-A'. The shear webs transfer load between the PS and SS surfaces and resist buckling. The spars along with the LE and aft shear webs form a box-type beam structure that withstands mainly bending, while the remaining construction preserves the blade shape responsible for its aerodynamic performance. The blade exhibits a maximum chord length of 7.63 m, which is located at a distance of 19.5 m from the root. At the root of the blade, there is a maximum twist angle of 13.3 degrees. The thickness of the blade varies throughout its length and is dependent on the type of airfoil employed at different locations span-wise.

The composite layup of the blade comprises Eglass/epoxy, where UD laminates are utilized for the spars and TE reinforced panel regions. The root buildup consists of tri-axial (TX) laminates, while the external and internal skins of the blade incorporate 5-mm-thick TX laminates. Sandwich constructions, made by combining foam and skins, are used to build the LE, aft and TE reinforced panel regions. For webs, sandwich
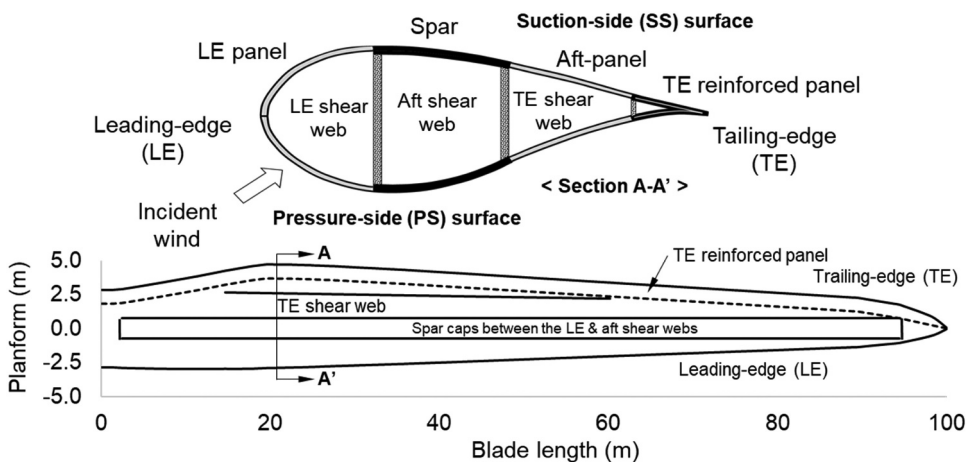

Figure 1. The SNL100–00 blade's planform along with a cross-section view A-A'.

Table 1. Mechanical properties of materials used in the layup [29].

Material description	Density (kg/m^3)	Stiffness				Strength	
		E_L (GPa)	E_T (GPa)	v_{LT} (-)	G_{LT} (GPa)	ε_{max} (%)	ε_{min} (%)
UD laminate (E-LT-500/ EP-3): $[0]_2$	1920	41.8	14.0	0.28	2.63	2.44	−1.53
BX laminate (Saertex/ EP-3): $[\pm45]_4$	1780	13.6	13.3	0.51	11.8	2.16	−1.80
TX laminate (SNL Triax): $[0]_2[\pm45]_2$	1820	27.7	13.65	0.39	7.2	-	-
Gelcoat	1235	3.44	3.44	0.3	1.38	-	-
Resin (EP-3)	1100	3.5	3.5	0.3	1.4	-	-
Foam	200	0.256	0.256	0.3	0.022	-	-

constructions made of 3-mm-thick biaxial (BX) laminates $[\pm45]_4$ and foam are employed. The blade features a protective gelcoat layer of 0.6 mm thickness, and an extra resin layer is also added to ensure that the blade mass is realistic. Table 1 lists the longitudinal stiffness (E_L), transverse stiffness (E_T), Poisson ratio (v_{LT}), and shear stiffness (G_{LT}) properties of the layup materials used. The ultimate tensile and compressive strains of the material are represented by ε_{max} and ε_{min}. Additional information about the geometry and layup of the blade can be found in [29].

3. Design requirements

The design of a wind turbine blade must account for a wide range of conditions that the turbine may encounter over its operational lifespan. To ensure structural integrity in terms of stiffness, strength, stability, and fatigue design requirements, the International Electrotechnical Commission (IEC) standard 61,400–1 defines 22 design load conditions (DLCs) that encompass various external factors such as wind and electrical conditions [9].

For the SNL100–00 blade, the stiffness and strength design requirements govern the design [29] as it generates the worst loads for a stationary and a spinning blade respectively, so the relevant DLCs 6.2 and 1.4 were chosen for optimization. The DLC 6.2 describes an abnormal condition of electrical grid power loss accompanied with a failure of pitching the blades out of extreme steady-state wind represented with a 50-year extreme wind model that causes the highest tip deflection and strains for the zero-degree pitched stationary rotor blades. While the DLC 1.4 describes a normal power production condition of the spinning rotor blades subjected to an extreme coherent wind gust with a direction change that causes the highest tip deflection and strains.

4. Modelling and verification

The model of the SNL100–00 blade, as depicted in Figure 2(a), was prepared using an open-source tool called Co-Blade. The stiffness, strength, and stability analyses were performed by calculating the tip deflection, strains, and buckling resistance.

The Co-Blade analysis tool is programmed in MATLAB and is used to analyse composite beam structures [30]. It utilizes classical laminate theory of composites, the Euler–
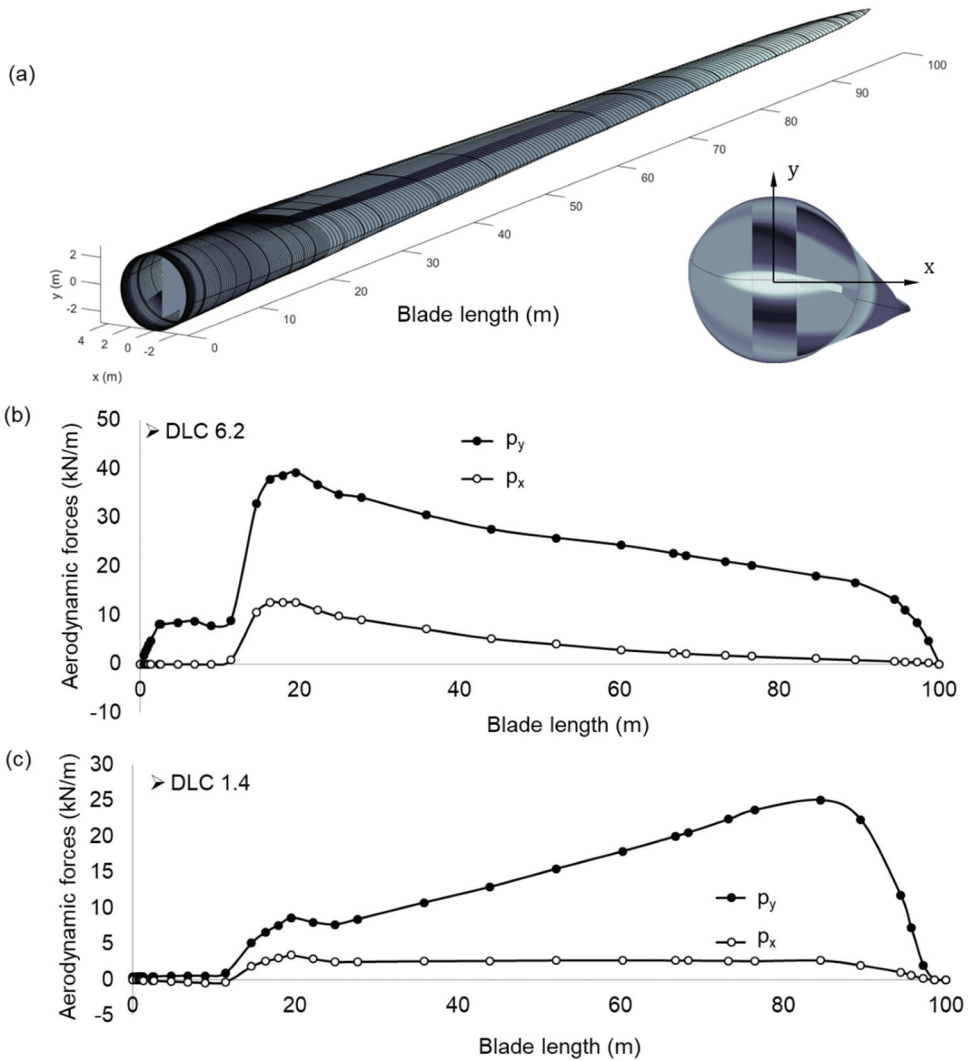
Figure 2. (a) The model of SNL 100–00 blade generated from Co-blade, and the computed wind loads for (b) a zero-degree pitched stationary blade, and (c) a spinning blade at rated 7.44 rpm.

Bernoulli beam theory, and considers transverse and torsional cross-sectional shear flows. In case of buckling, it idealizes the composite panels of the beam structures as isotropic plates pinned supported on all edges which is a simple yet conservative boundary condition likely to overdesign the panel thickness. It should be noted that the Co-Blade cannot perform modal analysis, however, it can be linked with a program BModes [31] that computes the mode shapes and natural frequencies of stationary as well as rotating Euler–Bernoulli beam with zero damping by solving relevant coupled partial differential equations. Consequently, the natural frequencies of the parked and the spinning SNL100–00 blades were estimated from BModes to check the potential resonance. Figure 2(b,c) shows computed flap-wise and edge-wise wind loads, denoted by p_y and p_x respectively, acting on the blade aerodynamic center. The loads were computed from blade element momentum (BEM) theory that considers the

blade aerodynamic shape [32]. For both DLCs, the magnitude of flap-wise load which causes the blade bending was higher than that of the edge-wise load. The inboard of the parked blade experienced the highest flap-wise load for DLC 6.2, primarily due to the drag forces caused by wind, while the outboard of the rotating blade experienced the highest flap-wise load for DLC 1.4, primarily due to wind-induced lift forces. The computed loads were used not only to verify the blade model but also used for the spar optimization.

Before optimization, the blade model was verified. The computed mass estimated to be 112,112 kg as listed in Table 2, was 1.8% lower than the reported value of 114,172 kg in [29], showing a good agreement. Further, the mass breakdown shows that the UD spars contribute almost 37% to the blade mass, clearly presenting a mass saving opportunity if the spar thickness is optimized.

Figure 3(a) shows that the blade deflection estimated for the DLC 6.2. The computed tip deflection of 12.04 m of the parked blade was in a good agreement with that of the reported value of 12.3 m in [29]. Likewise, the computed tip deflection of 11.84 m of the spinning blade for the DLC 1.4 was also in a good agreement with that of the reported value of 11.9 m in [29] but is not shown for brevity. Figure 3(b) shows the span-wise peak longitudinal strains for the blade PS and SS estimated for the DLC 1.4. The PS peak strains were tensile and that of the SS were compressive, demonstrating a typical bending behaviour. The highest tensile peak strain of 3,660 microns occurred at the 54.5 m span on the PS and the highest compressive strain of 3,567 microns occurred at the 66.5 m span on the SS. The computed and reported values of PS peak strains at the blade root were close to each other, however a discrepancy was observed at the blade span of 19.5 m where the computed PS peak strain from Co-Blade was almost 18% higher than that reported in [29]. This discrepancy can be attributed to different methodologies used to estimate peak strain in Co-Blade and that used by Griffith [29]. Further, two strain spikes, represented by symbols A and B in Figure 3(b), were observed which were caused by abrupt changes in the layup thickness. The strain spike A at the blade span of 1.3 m occurred where the thickness of the foam core begins in the layup of the LE and aft panel regions, and the strain spike B at the blade span of 14.6 m occurred where the thickness of TX root buildup ends. The presence of strain spikes shows the need to optimize the blade composite layup, particularly the root buildup region, so such an attempt was made as the current scope is limited to the blade spar optimization only. Similar findings for the blade PS and SS peak longitudinal strains were also observed for DLC 6.2 but are not discussed to avoid repetition. Figure 3(c) shows the buckling results estimated for DLC 6.2. The computed lowest bucking load factor of 2.374 was located at a distance of 78 m from the blade root, which is in good agreement with that of the reported value of 2.229 in [29]. Moreover, the computed lowest mode frequency of the fixed base of

Table 2.   Mass breakdown of the SNL100–00 blade model.

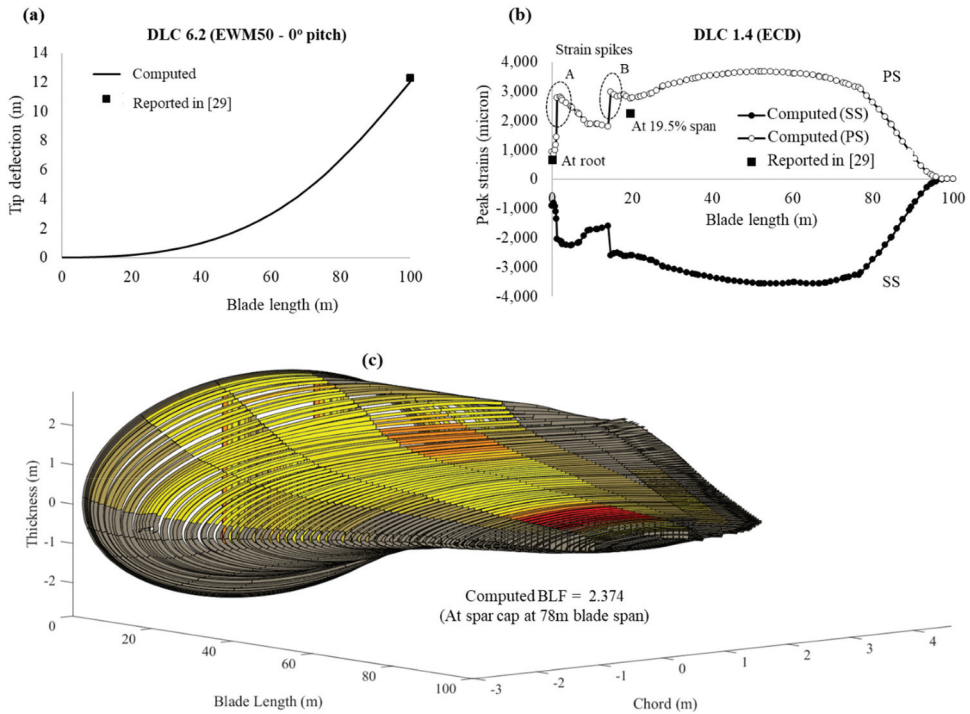| Layup material	Mass breakdown	
	kg	%
UD (PS & SS spars)	41,637	37.1
UD (TE reinforcement)	7,782	6.9
BX (Web skins)	3,505	3.1
TX (PS & SS skins)	22,476	20.0
TX (Root build-up)	15,274	13.6
Others (Gelcoat, extra resin, foam)	21,438	19.1
Total	112,122	100

Figure 3. The computed results for model verification: (a) tip deflection, (b) the span-wise distributions of PS and SS peak longitudinal strains, and (c) buckling resistance.

blade computed from BMode was 0.45 Hz, which is in good agreement with the reported value of 0.42 hz in [29].

5. Optimization formulation

Optimization of the spar thickness to achieve blade mass reduction is a challenging task that requires a multi-criteria approach, with all design requirements specified by the wind turbine standards being met for each potential solution in the design space. This work considers blade stiffness, strength, buckling, and vibration design requirements during the optimization process. However, fatigue design requirements are not considered due to their complexity and the computational cost involved. Additionally, fatigue is not a key factor driving the design of the SNL100–00 blade [29]. It is expected that blade fatigue performance will improve following the mass reduction since gravity-induced loads are the main cause of edge-wise fatigue in large-scale blades.

The spar thickness optimization for the SNL100–00 blade for the DLCs 6.2 and 1.4 was carried out considering 03 cases listed in Table 3. For cases 1 and 2, the spar optimization was conducted for the DLCs 6.2 and 1.4, respectively. For case 3, the optimization problem was solved while simultaneously meeting the design requirements for both the DLCs 6.2 and 1.4.

Table 3. List of the optimization cases.

Case #	Design load cases (DLCs)
Original	6.2 and 1.4
1	6.2
2	1.4
3	6.2 and 1.4

5.1. *Objective function*

For the spar thickness optimization, the blade mass objective function $F(x_i)$ was expressed by Eq. 1.

$$F(x_i) = \sum \rho_i V_i \qquad (1)$$

Where x_i, ρ_i and V_i represent the design variables to formulate the optimization problem and densities and volumes of the materials used in the blade layup, respectively.

5.2. *Design variables*

The distribution of blade spar thickness along the span of the blade is presented in Figure 4(a). The spar thickness is achieved by sequentially stacking unidirectional (UD) plies to reach the desired thickness and extends across nearly the entire span of the blade. At the root of the blade, the thickness is zero and progressively increases. At a span of 19.5 m, it reaches a maximum value of 136 mm before remaining constant until 24.9 m. Beyond this point, the thickness gradually decreases until it reaches zero at the blade tip.

To perform optimization, the distribution of spar thickness and the corresponding locations along the blade span were represented using 14 design variables, denoted by x_i, as shown in Eq. 2.

$$x_i = [x_1, x_2, x_3, \ldots, x_{14}]^T \qquad (2)$$

Where eight discrete design variables (i.e. x_1 to x_8) describe the thicknesses while the remaining six continuous variables (i.e. x_9 to x_{14}) describe locations along the blade span as shown in Figure 4(b). The thickness variables in particular were selected in such a manner that they covered most of the spar thickness. The variables x_1 to x_4 were used to represent the increasing spar thickness at the inboard and the variables x_5 to x_8 were used to represent the decreasing spar thicknesses at the outboard, while the constant spar thickness was represented by the variables x_4 and x_5.

It should be noted that the both PS and SS spars were defined by the same design variables, and that the values between two design variables were linearly interpolated, and that the computed wind loads were applied at the blade pitch-axis and were assumed to be unaffected during optimization.
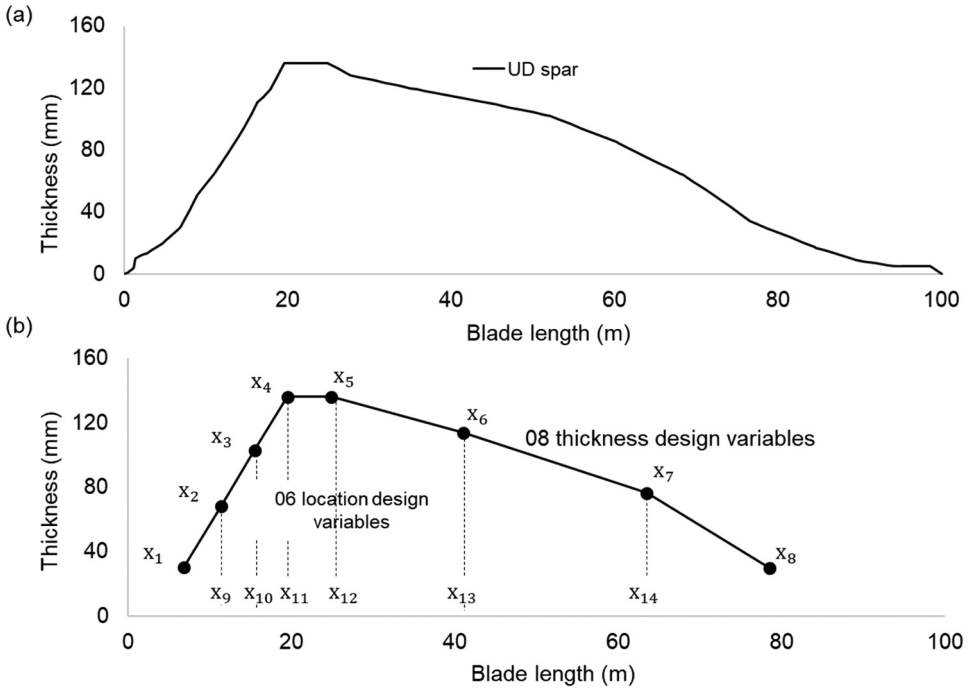
Figure 4.   For the blade UD spars: (a) the thickness distribution in the span-wise direction, and (b) its discrete representation using design variables.

5.3.   *Constraints*

5.3.1.   *Stiffness*

This constraint ensures that the blade does not collide with the tower and can be written as $\delta \leq \delta_{allow}$, where δ is computed blade tip deflection resulting from the incident wind loads for the DLCs 6.2 and 1.4, and δ_{allow} is allowable clearance between the blade and the tower. For the 13.2 MW wind turbine, a total blade-tower clearance of 19.54 m was determined using various parameters, including the tower height of 142.2 m, tower radius of 2.0 m, hub radius of 2.5 m, shaft overhang of 8.16 m, shaft tilt of 2.5 degrees, and blade pre-cone angle of 2.5 degrees [29]. According to the wind turbine standard [10], a minimum blade-tower clearance of 5% is required for a stationary rotor, and 30% for a rotating rotor. Consequently, for DLCs 6.2 and 1.4, estimated values of 18.56 m and 13.68 m were determined for δ_{allow}, respectively.

5.3.2.   *Strength*

To prevent blade strength failure due to incident wind loads, this constraint is written as $\varepsilon \leq \varepsilon_{allow}$, where ε represents the maximum peak longitudinal strain along the PS and SS surfaces of the blade, and ε_{allow} represents the allowable strain. The ε_{allow} is determined by considering the ultimate strain value of each material utilized in the layup and adjusting for the load and material reduction factors specified in the wind turbine standard [10]. The load reduction factor is

used to account for uncertainties related to loads, whereas the material reduction factor considers the impact of aging, environment, and manufacturing method. For strength analysis, the $\varepsilon_{\text{allow}}$ values for the UD and BX laminates were considered as these laminates mainly contribute to the blade strength response.

5.3.3. *Buckling*

To prevent blade buckling failure, the constraint is expressed as $\lambda \leq 1$, where λ represents the ratio of load-induced stresses to the critical buckling stresses, as expressed by Eq. 3. For a safe design, λ must be less than 1.

$$\lambda = \left(\sigma_c/\sigma_{c,\text{crt}}\right)^a + \left(\tau/\tau_{\text{crt}}\right)^b \tag{3}$$

where the load-induced in-plane compressive normal and shear stresses are represented by σ_c and τ, respectively. While, $\sigma_{c,\text{crt}}$ and τ_{crt} denote the critical in-plane compressive normal and shear stresses causing buckling. The values of $\sigma_{c,\text{crt}}$ and τ_{crt} were computed for the PS and SS composite panels as well as for the shear web panels, from Co-Blade tool using the material properties and panel geometries. As per the wind turbine standard [10], a material reduction factor of 2.042 was applied to the skin laminates, while a factor of 1.856 was applied to the foam core, to estimate the critical buckling stresses. For the PS and SS panels, exponents a and b were assigned values of 1 and 1.5, respectively, while values of 2 and 2 were assigned to the shear web panels.

5.3.4. *Modal*

This constraint ensures that the natural frequency of the blade should not coincide with the rotational speed of the turbine to avoid resonance, and is expressed $|f_1 - f_R| \geq \Delta$, where f_1 refers to the first natural frequency of the blade, f_R refers to the rotational frequency of the turbine, and Δ represents the difference between f_1 and f_R. For resonance analysis, the value of f_R was set to 0.124 hz, derived from the rated 7.44 rpm of the spinning rotor of the turbine. Additionally, a value of 0.3 hz was assigned to Δ.

5.3.5. *Constraints on design variables*

To ensure an optimal design that considers manufacturing and material continuity, following constraints were placed on the design variables, limiting the design space. The constraints on the 08 discrete thickness design variables (i.e. x_1 to x_8) and 06 location variables (i.e. x_9 to x_{14}) were expressed by Equation 4 and 5, respectively.

$$\left.\begin{array}{r}x_{j+1} - x_j \geq 0, (j = 1, 2, 3) \\ x_4 - x_5 = 0 \\ x_k - x_{k+1} \geq 0, (k = 5, 6, 7)\end{array}\right\} \tag{4}$$

$$x_{m+1} - x_m \geq 0, (m = 9, 10, 11, \ldots, 13) \tag{5}$$

Finally, the bound constraints on all 14 design variables were expressed by Eq. 6.

Table 4. Design variables, constraints and bounds used for the optimization.

Parameter	Lower bound	Upper bound	Units
$x_1 - x_8$	10	136	mm
$x_9 - x_{14}$	6.8	78.5	m
δ	-	13.68 for DLC1.4 18.56 for DLC6.2	m
ε	-	+8,196, −5,139 (UD laminate) +7,256, −6,046 (BX laminate)	micron
λ	-	1	-
f_1		$\leq f_r - 0.3$ or $\geq f_r + 0.3$	Hz

$$x_i^L \leq x_i \leq x_i^U, (i = 1, 2, 3, \ldots, 14) \tag{6}$$

Where the bounds (i.e. lower and upper) on the design variables x_i are represented by x_i^L and x_i^U. All bounds and constraints used to ensure the feasible design space are summarized in Table 4.

5.4. *Genetic algorithm method*

For the spar optimization, the genetic algorithm (GA) method was used. The method imitates the process of natural selection observed in the biological sciences and is widely adopted by the research community to solve multi-constrained optimization problems in the field of composite structures [33–35]. It is a population-based stochastic search algorithm well suited for mixed-integer optimization problems, achieving global convergence through mechanisms such as random search, crossover, and mutation among population members.

Figure 5 shows a generic flowchart of the GA optimization method. The algorithm starts off with an initial population comprising many individuals that define the blade spar. Afterward, a fitness function is estimated for each individual that describes the objective function and relevant constraints. The evaluation of fitness function requires to perform the blade stiffness, strength and buckling analyses using Co-Blade and the blade resonance analysis using BModes program. The value of the fitness function is utilized to choose individuals as parents for generating offspring in the subsequent generation. The principles of natural selection, cross-over, and mutation are applied to produce offspring. The iterative process stops when the maximum number of generations is reached, and an optimized solution is obtained.

In the MATLAB environment, the optimization process was carried out utilizing the GA function [36] provided by the software. The number of individuals and generations was set to 20 and 250, respectively, after several trials. The default crossover and mutation probabilities of 0.8 and 0.01 were applied to the population. For integer variables, the 'INTCON' option, which specifies the index vector for the integer variables, was used.

To optimize the use of GA, a fitness function was formulated, as shown in Equation 7, which combines the objective function with different penalty factors accounting for design constraints.

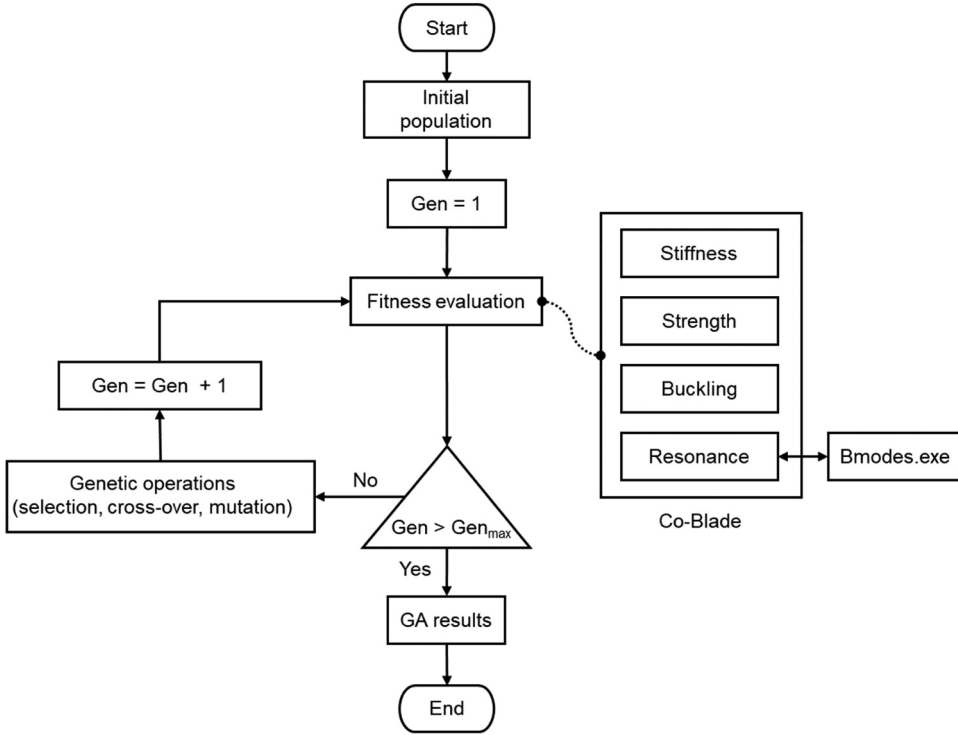$$\min F(x_i) = \text{Blade mass} \times \prod max(1, p_n)^2$$

Figure 5.   Schematic presenting the process of optimizing using genetic algorithm (GA).

$$p_1 = \delta/\delta_{\text{allow}}, \, p_2 = \varepsilon/\varepsilon_{\text{allow}}, \, p_3 = \lambda, \, p_4 = \Delta/|f_1 - f_r| \tag{7}$$

where p_n represents the penalty factors to be defined in proportion to the constraint violations or equal to 1 otherwise. To minimize the fitness function, the blade mass should be minimized while ensuring that all penalty factors remain less than or equal to 1.

6.   Results and discussion

Figure 6 presents a comparison of the convergence histories of the blade mass for the optimization cases outlined in Table 3, following the completion of 250 generations. Case 1 achieved the lowest blade mass of 100,940 kg, which could be further reduced by increasing the number of iterations, as no bound or constraint was violated. However, considering the increased computational cost and the lack of significant mass savings, the existing optimized result can be deemed satisfactory. In cases 2 and 3, the blade mass was decreased to 103,300 kg and 103,376 kg, respectively. However, the margin to achieve the permissible tip deflection of 13.68 m for DLC 1.4 was fully utilized, restricting further reductions in mass. Therefore, a blade mass reduction of 10.37% for case 1 and almost 7.8% for cases 2 and 3 was achieved.

A comparison between the original and optimized UD spars is presented in Figure 7. Overall, the highest spar thickness for the original design decreases in all cases and tends to shift towards the middle span of the blade. The solid line with filled circular markers
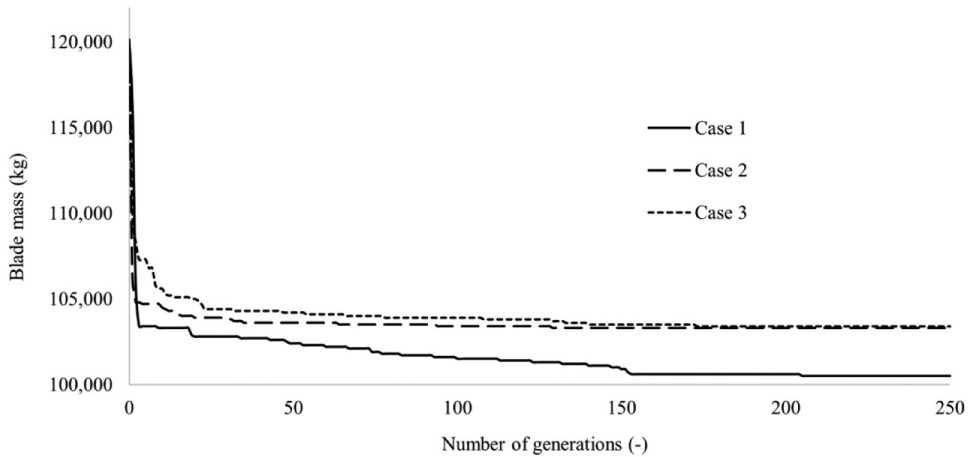
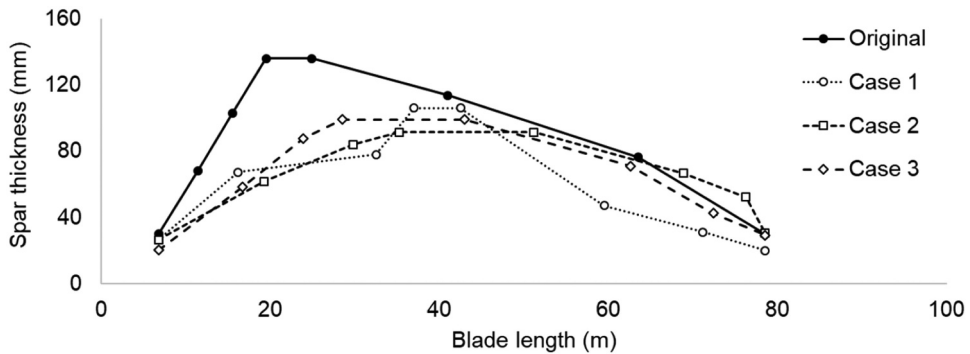Figure 6.   The histories of the blade mass convergence.

Figure 7.   Comparison of the optimized UD spars.

represents the highest thickness of the original spar, which is 136 mm at the span between 19.5 m and 24.9 m. In case 1, the optimized spar thickness is depicted by a dotted line with hollow circular markers, which increases near the blade span of 16 m and decreases at the blade span of 60 m and beyond until the blade tip is reached. The highest spar thickness of 106 mm is observed at the blade span between 37 m and 42.5 m. It appears that the optimization algorithm aims to increase the spar thickness at the inboard and decrease it at the outboard, which is consistent with the highest flap-wise wind load causing bending occurring at the blade inboard region for DLC 6.2, as shown in Figure 2(b).

For case 2, the optimized spar thickness, represented by a short-dash line with square markers, decreases at the blade span between 19.3 m and 30 m and increases at the blade span of 51.2 m and beyond, while the highest spar thickness of 91.4 mm occurs at the blade span between 35.3 m and 51.2 m. In this case, the algorithm attempts to decrease the spar thickness at the inboard and increase at the outboard which in line with the fact that for DLC 1.4, the highest flap-wise wind load causing bending occurs at the blade outboard region as shown in Figure 2(c). Finally, for case 3, the optimized spar thickness is represented by a long-dash line with rotated square

Table 5. Summary of optimization results.

Case #	Blade mass (kg)	DLC #	Tip deflection (m)	Max. peak longitudinal strain (micron)	Buckling criterion (-)	1st natural frequency (Hz)
Original	112,200	6.2	12.37	4,188 (PS at 1.30 m)	0.379 (SS at 76.5 m)	0.45
		1.4	11.84	3,843 (PS at 54.4 m)	0.376 (SS at 76.5 m)	
1	100,490 (10.37% reduction)	6.2	16.07	5,513 (PS at 19.5 m)	0.656 (SS at 68.3 m)	0.423
		1.4	13.68	5,134 (PS at 19.5 m)	0.472 (SS at 19.5 m)	
2	103,300 (7.8% reduction)	6.2	14.20	5,768 (PS at 14.6 m)	0.827 (SS at 14.5 m)	0.406
3	103,376 (7.8% reduction)	1.4	13.68	4,758 (PS at 17.0 m)	0.684 (SS at 14.5 m)	0.412

markers. For this case, the algorithm attempts to satisfy both DLCs 6.2 and 1.4, consequently the spar thickness increases at the blade inboard and outboard regions, while the highest thickness of 99 mm appears at the blade span between 28.5 m and 43.0 m. Further, it can be clearly observed from Figure 7 that the peak UD spar thickness for the original design that lies nearly at the one quarter of the blade length is shifted to almost mid of blade length after optimization.

Table 5 provides a summary of the optimization outcomes. A reduction in blade bending stiffness due to the thinning of spars resulted in a decrease in tip deflection for all cases. Cases 2 and 3 attained the global optimum solutions by attaining the permissible tip deflection limit of 13.68 m. For all cases, the highest longitudinal strains were consistently tensile and localized on the blade PS spar. Optimization caused a spike in peak strains, but they remained below the allowable limits. The highest tensile peak strain occurred for DLC 6.2 in the UD laminates at the 14.6 m span of the PS spar, measuring 5,768 microns. The buckling criterion increased in all cases due to the reduction in spar thickness, but the allowable limit was not exceeded. The highest buckling was observed at the blade SS spar in case 1 and at the outboard region in cases 2 and 3. At the SS spar at 14.5 m span, the highest buckling criterion of 0.827 was recorded. As a result of the decrease in blade mass and structural stiffness, the first natural frequency decreased in all cases. However, the reduction in structural stiffness was greater than the reduction in blade mass, resulting in a decrease in the first natural frequency. Case 2 had the lowest natural frequency of 0.406 hz, which was well below the resonance frequency of 0.124 hz, indicating no danger of resonance. The optimization achieved a blade mass reduction of 7.8–10.37% while fulfilling all the design requirements, thus demonstrating better use of UD laminates in the blade spars.

7.   Conclusions

The UD spars of the publicly available SNL100–00 blade, designed for the future generation of multi-MW wind turbine with a rated power of 13.2 MW, were optimized for thickness to reduce mass. The GA optimization method was employed to optimize the spar while satisfying the design requirements for stiffness, strength, buckling, and resonance for DLCs 6.2 and 1.4, which produce the most challenging wind loads for parked and rotating rotors at rated 7.44 rpm. The optimization problem was simplified by keeping the remaining blade layup unchanged, making it more economical to solve.

Since the UD spars account for almost 37% of the blade mass, adjusting their thickness provides an opportunity for mass savings. Three optimization scenarios were examined as specified in Table 3. In case 1, a reduction in mass by 10.37% was demonstrated, whereas cases 2 and 3 exhibited only a 7.8% reduction in mass due to the limit imposed by the tip deflection restriction of 13.68 m for DLC 1.4. As a result, further reduction was constrained. The tip deflection and peak longitudinal strains increased, while the buckling resistance and the first natural frequency decreased for all cases, but no resonance occurred, demonstrating effective utilization of UD laminates in blade spars that can benefit from a manufacturing perspective.

Although this study focused on UD spar optimization for the SNL100–00 blade, there is room for improvement in the remaining composite layup, particularly at the blade root region, where strain spikes were observed due to abrupt variations in layup thickness. Additionally, the blade topology needs refinement.

ORCID

Suhail Attar http://orcid.org/0000-0003-4155-5734

Author contributions

Conceptualization, K.H.; methodology, K.H.; software, K.H.; verification, K.H.; formal analysis, K.H.; investigation, K.H.; resources, S.A.; writing – original draft preparation, K.H. and S.A.; writing – review and editing, K.H. and S.A.; visualization, K.H. and S.A.; supervision, K.H. and S. A.; project administration, S.A. All authors have read and agreed to the published version of the manuscript.

References

[1] Wiser R, Bolinger M, Hoen B, et al. Land-based wind market report: 2023 edition. 2023.
[2] Musial W, Spitsen P, Duffy P, et al. Offshore wind market report: 2023 edition. Golden (CO): National Renewable Energy Laboratory (NREL); 2023.
[3] Bilgili M, Alphan H. Global growth in offshore wind turbine technology. Clean Technol Environ Policy. 2022;24(7):2215–2227. doi: 10.1007/s10098-022-02314-0
[4] Blom R, Bortolotti P, Griffith T, et al. (Chris) 50 MW segmented ultralight morphing rotors for wind energy. Charlottesville (VA): University of Virginia; 2024.
[5] Jeong M, Loth E, Qin C, et al. Aerodynamic rotor design for a 25 MW offshore downwind turbine. Appl Energy. 2024;353:122035. doi: 10.1016/j.apenergy.2023.122035
[6] Li C, Mogollón JM, Tukker A, et al. Future material requirements for global sustainable offshore wind energy development. Renew Sustain Energy Rev. 2022;164:112603. doi: 10. 1016/j.rser.2022.112603
[7] Griffin DA. Cost/Performance tradeoffs for carbon fiber in wind turbine blades. In: Proceedings of the Sandia Blade Technology Workshop, Albuquerque, New Mexico, USA; 2004.
[8] Trends in the design, manufacture and evaluation of wind turbine blades - veers - 2003 - wind energy - Wiley online library available online. [cited 2024 Sep 19]. Available from: https:// onlinelibrary.wiley.com/doi/abs/10.1002/we.90
[9] IEC. 61400–1. Wind turbines part 1: design requirements. Int Electrotech Comm. 8621 (3):177.
[10] Lloyd G, Hamburg G. Guideline for the certification of offshore wind turbines. 2005.
[11] Monte AD, Raciti Castelli M, Benini E. Multi-Objective Structural Optimization of a HAWT Composite Blade. Compos Struct. 2013;106:362–373. doi: 10.1016/j.compstruct.2013.05.038
[12] Hu W, Han I, Park S-C, et al. Multi-objective structural optimization of a HAWT composite blade based on Ultimate Limit State Analysis. J Mech Sci Technol. 2012;26(1):129–135. doi: 10.1007/s12206-011-1018-3

[13] Hu W, Park D, Choi D. Structural optimization procedure of a composite wind turbine blade for reducing both material cost and blade weight. Eng Optim. 2013;45(12):1469–1487. doi: 10.1080/0305215X.2012.743533

[14] Zhu J, Cai X, Pan P, et al. Optimization design of spar cap layup for wind turbine blade. Front Struct Civ Eng. 2012;6(1):53–56. doi: 10.1007/s11709-012-0147-9

[15] Liao CC, Zhao XL, Xu JZ. Blade layers optimization of wind turbines using FAST and Improved PSO algorithm. Renew Energy. 2012;42:227–233. doi: 10.1016/j.renene.2011.08.011

[16] Cai X, Zhu J, Pan P, et al. Structural optimization design of horizontal-axis wind turbine blades using a particle swarm optimization algorithm and finite element method. *Energies*. 2012;5(11):4683–4696. doi: 10.3390/en5114683

[17] Zhu J, Cai X, Pan P, et al. Multi-objective structural optimization design of horizontal-axis wind turbine blades using the non-dominated sorting genetic algorithm II and Finite element method. *Energies*. 2014;7(2):988–1002. doi: 10.3390/en7020988

[18] Albanesi AE, Peralta I, Bre F, et al. An optimization method based on the evolutionary and topology approaches to reduce the Mass of composite wind turbine blades. Struct Multidiscip Optim. 2020;62(2):619–643. doi: 10.1007/s00158-020-02518-2

[19] Hermansen SM, Lund E. Multi-material and thickness optimization of a wind turbine blade root section. Struct Multidiscip Optim. 2024;67(7):1–24. doi: 10.1007/s00158-024-03811-0

[20] Van Dam CP, Mayda E, Chao D, et al. Innovative structural and aerodynamic design approaches for large wind turbine blades. In: Proceedings of the 43rd AIAA Aerospace Sciences Meeting and Exhibit; Reno (NV): American Institute of Aeronautics and Astronautics; 2005 Jan 10.

[21] Grujicic M, Arakere G, Pandurangan B, et al. Multidisciplinary design optimization for glass-fiber epoxy-matrix composite 5 MW horizontal-axis wind-turbine blades. J Mater Eng Perform. 2010;19(8):1116–1127. doi: 10.1007/s11665-010-9596-2

[22] Fischer GR, Kipouros T, Savill AM. Multi-objective optimisation of horizontal axis wind turbine structure and energy production using aerofoil and blade properties as design variables. Renew Energy. 2014;62:506–515. doi: 10.1016/j.renene.2013.08.009

[23] Ashuri T, Zaaijer MB, Martins JR, et al. Multidisciplinary design optimization of large wind turbines—technical, economic, and design challenges. Energy Convers Manag. 2016;123:56–70. doi: 10.1016/j.enconman.2016.06.004

[24] Zhu J, Cai X, Gu R. Aerodynamic and structural integrated optimization design of horizontal-axis wind turbine blades. Energies. 2016;9(2):66. doi: 10.3390/en9020066

[25] Pourrajabian A, Nazmi Afshar PA, Ahmadizadeh M, et al. Aero-structural design and optimization of a small wind turbine blade. Renew Energy. 2016;87:837–848. doi: 10.1016/j.renene.2015.09.002

[26] Dal Monte A, De Betta S, Castelli MR, et al. Proposal for a coupled aerodynamic–structural wind turbine blade optimization. Compos Struct. 2017;159:144–156.

[27] Maheri A. Multiobjective optimisation and integrated design of wind turbine blades using WTBM-ANSYS for high fidelity structural analysis. Renew Energy. 2020;145:814–834.

[28] Shakya P, Thomas M, Seibi AC, et al. Fluid-structure interaction and life prediction of small-scale damaged horizontal axis wind turbine blades. Results Eng. 1467;23:102388. doi: 10.1016/j.rineng.2024.102388

[29] Griffith DT, Ashwill TD. The Sandia 100-meter all-glass baseline wind turbine blade: SNL100–00. Inf Téc Sandia Natl Lab. 2011. Available from: https://energy.sandia.gov/wp-content/gallery/uploads/113779.pdf.

[30] Sale D. User's Guide to Co-blade: software for structural analysis of composite blades. Northwest Natl Mar Renew Energy Cent. 4820. Available from: https://github.com/nnmrec/Co-Blade/blob/master/Documentation/Co-Blade%20Users%20Guide.pdf.

[31] Bir G. User's guide to bmodes (software for computing rotating beam-coupled modes) Golden (CO): National Renewable Energy Lab (NREL); 2005.

[32] Anderson C. *Wind turbines: theory and practice*. Cambridge, United Kingdom: Cambridge University Press; 2020.

[33] Corz A, Gomez-Ruiz JA, Pelaez JI, et al. Design and optimization of symmetric laminated composites using a variable neighbourhood search-based Model. Eng Optim. 2012;44 (4):505–520. doi: 10.1080/0305215X.2011.588225

[34] Naik GN, Gopalakrishnan S, Ganguli R. Design optimization of composites using genetic algorithms and failure mechanism based failure criterion. Compos Struct. 2008;83 (4):354–367. doi: 10.1016/j.compstruct.2007.05.005

[35] Liu BT, Haftka R, AAkgün M, et al. Permutation genetic algorithm for stacking sequence design of composite laminates. Comput Methods Appl Mech Eng. 2000;186(2–4):357–372. doi: 10.1016/S0045-7825(99)90391-2

[36] Chipperfield AJ, Fleming PJ. The MATLAB genetic algorithm toolbox. 1995.